Materials Physics and Mechanics. 2022;50(3): 431-438
Research article
http://dx.doi.org/10.18149/MPM.5032022_7

Submitted: October 17, 2022
Approved: October 31, 2022
Accepted: November 18, 2022

Grain-boundary nanoprecipitates-mediated mechanism of strengthening in Al-Cu-Zr alloy structured by high-pressure torsion

M.Yu. Gutkin[1], N.V. Skiba[2]✉, T.S. Orlova[2]

[1]Institute for Problems of Mechanical Engineering RAS, St. Petersburg, Russia

[2]Ioffe Institute, St. Petersburg, Russia

✉ nikolay.skiba@gmail.com

Abstract. The theoretical model is suggested which describes a new micromechanism of strengthening in the ultrafine-grained Al-Cu-Zr alloy subjected to severe plastic deformation. The departure point in this theoretical model is the assumption that the key role in the plastic deformation of high-pressure torsion processed ultrafine grained Al is played by extrinsic grain boundary dislocations (EGBDs) gliding along non-equilibrium grain boundaries and forming dislocation pile-ups at triple junctions of the grain boundaries. Within the model, nanoprecipitates of Al_2Cu at grain boundaries act as obstacles for the slip of extrinsic grain-boundary dislocations (EGBDs) that leads to a significant increase in the strength of the Al-Cu-Zr alloy. The plastic deformation occurs through the emission of lattice dislocations from the pile-up of EGBDs pressed to a triple junction of grain boundaries. It is shown that the division of gliding EGBDs into separate pile-ups by nanoprecipitates can provide substantial additional hardening of the alloy. The proposed model is in good quantitative agreement with available experimental results.

Keywords: ultrafine-grained aluminum alloys; grain boundary defects; precipitation; dislocations; plastic deformation

Acknowledgements. *Grant of the Russian Science Foundation (grant №22-19-00292).*

Citation: Gutkin MYu, Skiba NV, Orlova TS. Grain-boundary nanoprecipitates-mediated mechanism of strengthening in Al-Cu-Zr alloy structured by high-pressure torsion. Materials Physics and Mechanics. 2022;50(3): 431-438. DOI: 10.18149/MPM.5032022_7.

1. Introduction

Aluminum-based alloys exhibit high electrical conductivity and corrosion resistance. However, the modern practical applications of aluminum-based alloys also require high mechanical strength. One of the ways to substantially increase the strength of aluminum and Al-based alloys is the formation of ultrafine-grained or nanocrystalline structures through processing by severe plastic deformation (SPD) [1-4]. Alloying of aluminum with different doping elements such as copper (Cu) [5,6], magnesium (Mg) [7], zirconium (Zr) [8,9], etc also contributes to strength increase. It is well known that doping with copper leads to a refinement of the grain structure [10-12] and an increase in the strength [4,10] of aluminum-based alloys subjected to severe plastic deformation (SPD). For example, in a recent work [13], it is shown that Al-Cu-Zr alloy

structured by high-pressure torsion (HPT) demonstrates a significant increase in the strength characteristics while maintaining functional ductility and good electrical conductivity. The authors [13,14] observed the formation of individual Cu-containing nanosized precipitates – nanoprecipitates of the Al_2Cu secondary phase (Al_2Cu-NPs) with sizes of 20–40 nm at grain boundaries (GBs) as a result of HPT processing of Al-Cu-Zr alloy. According to [13], the formation of such Al_2Cu-NPs at GBs contributes to a significant increase in the strength of the Al-Cu-Zr alloy, which is hard to explain by known strengthening mechanisms. As was shown in [13], the value of such additional strengthening related to the Al_2Cu-NPs at GBs is about 130 MPa which is comparable with the contribution from GB strengthening to the total strength of this alloy.

The main aim of this work is to develop a theoretical model which would describe the strengthening mechanism in the Al-Cu-Zr alloy due to the Al_2Cu-NPs at GBs. In doing so, the departure point in this modeling is the assumption [15-18] that the key role in the plastic deformation of HPT processed ultrafine-grained (UFG) Al is played by extrinsic grain boundary dislocations (EGBDs) gliding along non-equilibrium GBs and forming dislocation pile-ups at triple junctions of the GBs. The critical stress required for the emission of lattice dislocations from the heads of such pile-ups to the bulk of neighboring grains was considered the flow stress of the UFG material [15-17]. With this assumption, some theoretical models were developed to explain the experimentally revealed effects of annealing-induced hardening [15,16] and deformation-induced softening [15,17] in HPT treated UFG Al, as well as the suppression of the annealing-induced hardening effect in it at low-temperature mechanical testing [18]. Since in the Al-Cu-Zr alloy structured in a similar HPT route, new important elements of the non-equilibrium GB structure – Al_2Cu-NPs – appear, one can expect their strong interaction with EGBDs and new significant features in the behavior of the latter. In the following section, we suggest a new theoretical model which reflects the interplay of EGBDs and Al_2Cu-NPs and allows us to estimate the contribution of Al_2Cu-NPs to the strengthening of the UFG Al-Cu-Zr alloy.

Model

Consider a single GB with an initial defect structure characterized by a pile-up of the EGBDs pressed by external shear stress τ to a triple junction of GBs (Fig. 1(a)). It is well known that such dislocation pile-up can emit lattice dislocations from the triple junction into the adjacent grain. Let an edge lattice dislocation with the Burgers vector $\mathbf{b}$ (hereinafter called b-dislocation) be emitted from the head of the dislocation pile-up under the action of the external shear stress τ and glide along a crystallographic plane that makes the angle α with the GB plane. In terms of the continuum approach, the emission of the b-dislocation can be represented as the formation of a dipole of the lattice dislocations with Burgers vectors $\pm\mathbf{b}$ (Fig. 1(a)).

According to our new model, the aforementioned Al_2Cu-NPs act as obstacles to the slip of the EGBDs. Thus, the appearance of the Al_2Cu-NPs in Al-Cu-Zr alloy structured by HPT leads to the formation of a new defect structure in the GB, which is characterized by N Al_2Cu-NPs periodically distributed along the GB with a period l, and $(N+1)$ identical pile-ups of EGBDs pressed by external shear stress τ to the NPs and to the triple junction of the GBs (Fig. 1(b)). For the sake of simplicity, the dislocation pile-ups at the NPs are modeled by edge superdislocations with Burgers vector $\mathbf{B}$ (hereinafter we call them B-superdislocations). The magnitudes of the superdislocation Burgers vectors are supposed to be the same, $B = nb_{gb}$, where n is the number of the EGBDs in each dislocation pile-up (Fig. 1(b)), and b_{gb} is the magnitude of the Burgers vector of an EGBD.

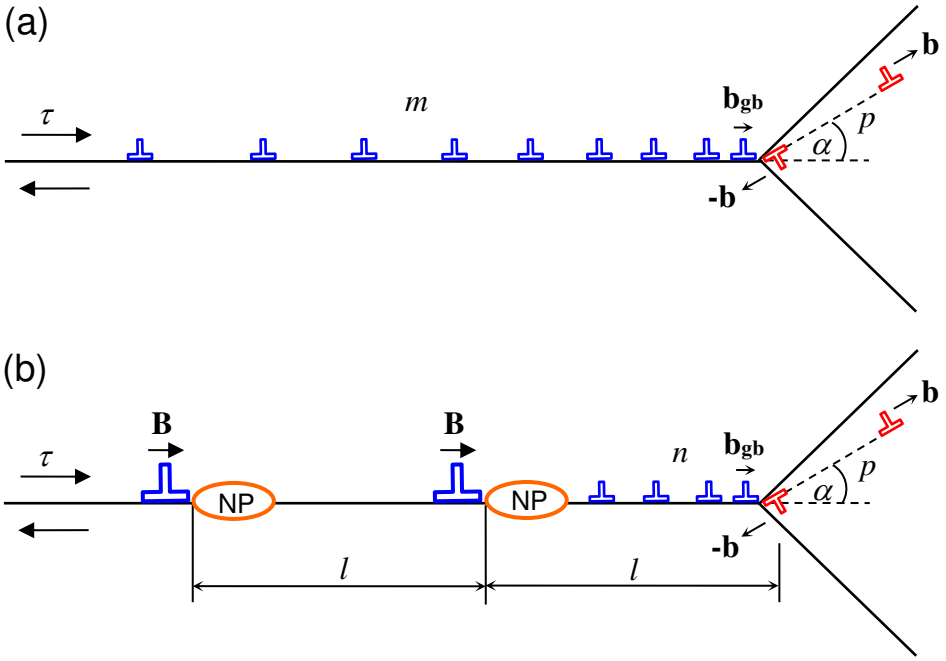

Fig. 1. Models of the lattice dislocation emission from the head of the pile-up of the EGBDs when (a) there are no NPs in the GB and (b) there are two NPs in the GB

Within the model, the combined action of the external shear stress τ and the shear stress field created by the superdislocations at the NPs leads to the emission of the lattice b-dislocation from the triple junction of the GBs. The emission event can be modeled as the formation of the corresponding $\pm b$-dislocation dipole (Fig. 1(b)).

Consider now the energy characteristics of the dislocation emission event illustrated in Fig. 1(b), and compare them with the energy characteristics of the dislocation emission from the head of the initial dislocation pile-up (Fig. 1(a)). In doing so, we will calculate the difference between the total energies characterizing the structure after and before the dislocation emission in the case shown in Fig. 1(b). The considered transformation of the defect system is energetically favorable if the total energy of the defect system decreases and energetically unfavorable if not.

The dislocation emission process is specified by the energy difference, $\Delta W = W_2 - W_1$, where W_1 is the energy of the initial state of the system before the dislocation emission and W_2 is the energy of the system after the dislocation emission (Fig. 1(b)). Such a transformation of the defect system is energetically favorable if $\Delta W < 0$.

The energy difference ΔW is determined by the expression:

$$\Delta W = E_{self}^{bb} + E_{\text{int}}^{B-bb} + E_{\text{int}}^{pu-bb} + E_{\text{int}}^{\tau}, \quad (1)$$

where E_{self}^{bb} denotes the self-energy of the $\pm b$-dislocation dipole, E_{int}^{B-bb} is the sum interaction energy of the B-superdislocations at the NPs, and the $\pm b$-dislocation dipole, E_{int}^{pu-bb} is the sum interaction energy between n EGBDs in the pile-up at the triple junction of the GDs and the $\pm b$-dislocation dipole, and E_{int}^{τ} denotes the interaction energy of the applied shear stress τ with the $\pm b$-dislocation dipole.

The self-energy E_{self}^{bb} of a dipole of $\pm b$-dislocations is given by the well-known formula [19]:

$$E_{self}^{bb} = Db^2\left(\ln\frac{p-r_c}{r_c}+1\right), \tag{2}$$

where $D = G/[2\pi(1-\nu)]$, G is the shear modulus, ν is the Poisson ratio, p is the dipole arm (in other words, it is the path moved by the emitted b-dislocation), and $r_c \approx b$ is the cut-off radius of the stress fields of the $\pm b$-dislocations.

To calculate the interaction energy between deferent defects, the standard procedure of calculating the work spent to nucleate a defect (or a group of defects) in the stress field of another defect (see, for example, [19] for details) was used. In doing so, according to Mura's method [20], the sum interaction energies E_{int}^{B-bb} and E_{int}^{p-bb} can be found using the following formulas, respectively:

$$E_{\text{int}}^{B-bb} = -\frac{DBb}{2}\sum_{i=1}^{N}\left(\cos\alpha\ln\frac{l_i^2+p^2+2l_i^2 p\cos\alpha}{l_i^2}-\frac{2l_i p\sin^2\alpha}{l_i^2+p^2+2l_i p\cos\alpha}\right), \tag{3}$$

$$E_{\text{int}}^{pu-bb} = -\frac{Db_{gb}b}{2}\sum_{i=1}^{n}\left(\cos\alpha\ln\frac{x_i^2+p^2+2x_i^2 p\cos\alpha}{x_i^2}-\frac{2x_i p\sin^2\alpha}{x_i^2+p^2+2x_i p\cos\alpha}\right), \tag{4}$$

where $l_i = il$, x_i are the positions of the EGBDs within the pile-up at the triple junction of the GBs (they are calculated as the roots of the first derivative of the Laguerre polynomial [21] within a special numerical iteration procedure described briefly below).

To determine the positions x_i of the EGBDs with taking into account the stress field of the B-superdislocations, the following numerical calculation algorithm was used. At first, the equilibrium positions of the EGBDs under the action of constant external shear stress τ only were calculated. Then they were recalculated with the account for the B-superdislocation stress effect. These corrected values of x_i were then used to find newly corrected values of the EGBD positions in the next iteration, and so on. This iteration procedure of subsequent corrections was performed until the values of x_i converge to some constant values.

The energy that specifies the interaction of the external shear stress τ with the lattice $\pm b$-dislocations is given by

$$E_{\text{int}}^{\tau} = -b\tau\, p\cos 2\alpha\ . \tag{5}$$

Results and Discussion

Let us analyze the dependences of the energy change ΔW on the characteristics of the system under consideration in the exemplary case of the UFG Al-Cu-Zr alloy with the average grain size $d \approx 300\,\text{nm}$ [13]. First, the dependences of ΔW on the distance p moved by the b-dislocation in the grain interior were calculated for different values of the external shear stress τ at the following typical values of the system parameters [22,23]: $G = 27\,\text{GPa}$, $\nu = 0.33$, $a = 0.405\,\text{nm}$, $b = a\sqrt{2}/2$, $b_{gb} = 0.1\,\text{nm}$, and $l = d/(N+1)$. The emission angle α was chosen as the average angle $\alpha = 22°$ between 0° and 45° that corresponds to the maximum and minimum levels of the external shear stress τ, respectively. The total number of EGBDs in all the cases under investigation is taken as $m = (N+1)n = 36$. This value well corresponds to the typical length of GBs in experiments [23,24] and allowed us to obtain the results that well meet the levels of the flow stress measured in [13]. The shear stress τ is related to the flow stress σ as follows: $\sigma = 2\tau/\cos 2\alpha$. The curves $\Delta W(p)$ are shown in Fig. 2 for different values of the flow stress σ at $n = 36$, 18, and 12 in the cases of no NPs ($N = 0$, Fig. 2(a)), one NP ($N = 1$, Fig. 2(b)), and two NPs ($N = 2$, Fig. 2(c)), respectively, in the GB that corresponds to direct experimental observations of Al_2Cu-NPs in [13].

In the case of no NPs ($N=0$, see Fig. 1a), the critical value of the flow stress $\sigma=\sigma_c$, under which the dislocation emission becomes energetically favorable ($\Delta W=0$ at $p=1$ nm and $\partial\Delta W/\partial p<0$ at $p>1$ nm), is equal to 320 MPa (see the red curve in Fig. 2(a)). Indeed, for $\sigma<\sigma_c$, there is an energy barrier for the emission (here it is ~1 eV/nm for $\sigma=220$ MPa, see Fig. 2(a)), while for $\sigma>\sigma_c$, there is no energy barrier and, moreover, $\Delta W<0$ and $\partial\Delta W/\partial p<0$ at $p\geq 1$ nm (see here the curve for $\sigma=420$ MPa in Fig. 2(a)).

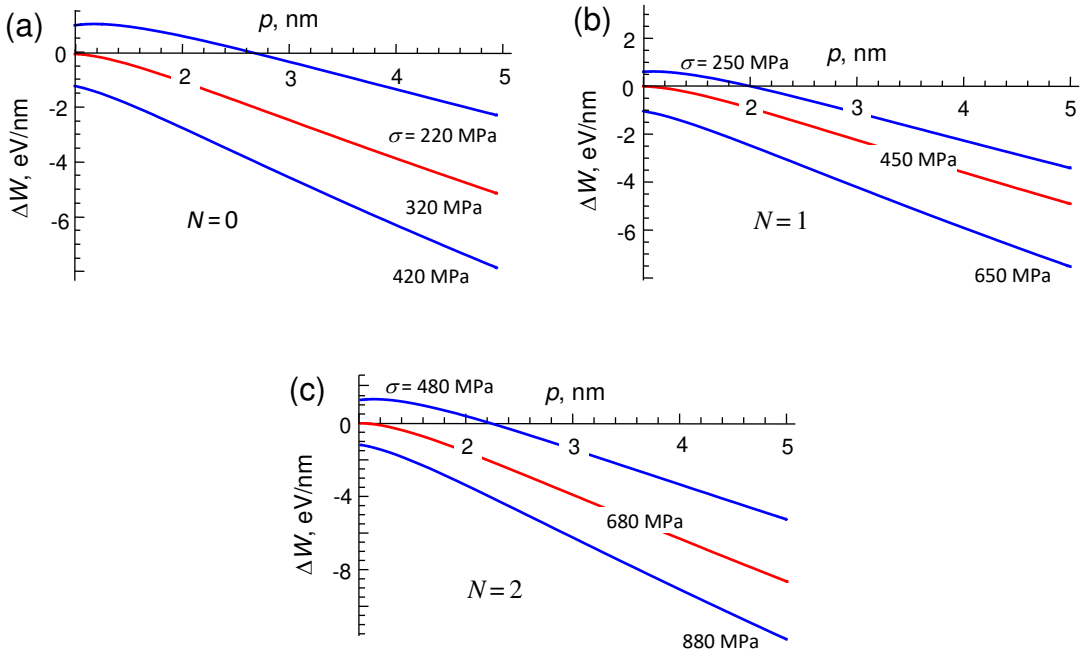

Fig. 2. Dependences of the energy difference ΔW on the distance p for different values of the flow stress σ and the number of the EGBDs in the pile-ups: (a) n=36, (b) 18, and (c) 12 in the cases of N=0, 1, and 2, respectively. The red curves correspond to the critical values of the flow stress under which the dislocation emission becomes energetically favorable

In the cases of one and two NPs ($N=1$ and 2, see Figs. 2(b,c)), the emission of lattice dislocations becomes energetically favorable at $\sigma\geq\sigma_c=450$ MPa and 680 MPa, respectively. To explain these results, we calculated the sum shear stress τ_{sum} in front of the pile-up, at $\alpha=0$ and at the distance 1 nm from the head EGBD – just in the emission region – for the three cases: (i) $N=0$, $\sigma=320$ MPa, (ii) $N=1$, $\sigma=450$ MPa, and (iii) $N=2$, $\sigma=680$ MPa. The results are $\tau_{sum}\approx 2.83$ GPa in case (i), 2.78 GPa in case (ii), and 2.79 GPa in case (iii) which is roughly 2.8 GPa in all three cases. This value is approximately equal to $G/10$ that is of the order of magnitude of the theoretical shear strength.

The dependence of the critical flow stress σ_c on the number N of the NPs in the GB is shown in Fig. 3. As is seen, σ_c noticeably increases with N and the discrete dependence $\sigma_c(N)$ is very close to linear. To determine the best-fitting line approximating our calculated points, we used the method of least squares. In the framework of this method, the equation of the best-fitting line for the dependence $\sigma_c(N)$ is given in units of GPa as follows:

$$\sigma_c\approx 0.255+0.235N. \qquad (6)$$

The corresponding linear dependence $\sigma_c(N)$ is shown by the solid line in Fig. 3. This result can be used for rough estimates of the expected yield stress of the UFG Al-Cu-Zr alloy with Al_2Cu-NPs in GBs, depending on the average number of nanoprecipitates at the boundary.

Thus, it is shown that, in the case of no NPs in GBs, the critical flow stress is about 320 MPa. It corresponds well to the value of the yield stress $\sigma_{0.2}$ estimated on the basis of experimentally determined microstructural parameters as the sum of contributions from known strengthening mechanisms, such as the Peierls-Nabarro hardening, the solid solution hardening, the strain hardening, the GB hardening and the dispersion hardening [13]. In contrast, in the case with one Al_2Cu-NP in a GB, it is about 450 MPa in accordance with measurements in Ref. 13. Therefore, the difference in 130 MPa can be attributed to the role of Al_2Cu-NPs as obstacles for the glide of EGBDs in non-equilibrium GBs typical for HPT processed metals and alloys. This difference characterizes the value of the additional hardening of the UFG Al-Cu-Zr alloy structured by HPT and demonstrates good agreement with experimental data [13]. It should be noted that in the HPT processed Al-Zr alloy, in which GBs did not contain any precipitates of secondary phase, the theoretically calculated value of $\sigma_{0.2}$ as the sum of known strengthening mechanisms well corresponds to the experimental value of the yield stress [24].

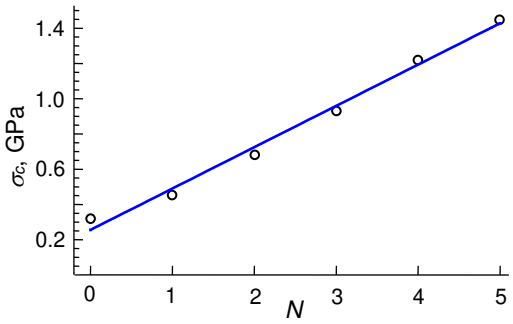

Fig. 3. Dependence of the critical flow stress σ_c on the number N of the NPs. The calculated points (open circles) are approximated by the best-fitting straight line

Summary and Conclusions

Thus, a theoretical model of a new micromechanism of strengthening in the UFG Al-Cu-Zr alloy is developed. In the model, the formation of Al_2Cu-NPs at GBs, which act as obstacles for EGBD slip, leads to a significant increase in the strength of the Al-Cu-Zr alloy. The deformation mechanism realizes through the emission of lattice dislocations from the heads of the pile-ups of the EGBDs near the triple junctions of the GBs. It is shown that the division of gliding EGBDs into separate pile-ups by Al_2Cu-NPs can provide additional hardening of the UFG Al-Cu-Zr alloy structured by HPT, the value of which well corresponds to experimental measurements [13].

References

1. Edalati K, Bachmaier A, Beloshenko VA, Beygelzimer Y, Blank V et al. Nanomaterials by severe plastic deformation: review of historical developments and recent advances. *Materials Research Letters*. 2022;10(4): 163-256.
2. Vu VQ, Toth LS, Beygelzimer Y, Zhao Y. Microstructure, texture and mechanical properties in aluminum produced by friction-assisted lateral extrusion. *Materials*. 2021;14(9): 246.
3. Horita Z, Tang Y, Masuda T, Takizawa Y. Severe plastic deformation under high pressure: upsizing sample dimensions. *Materials Transactions*. 2020;61(7): 1177-1190.
4. Xu W., Liu XC, Lu K. Strain-induced microstructure refinement in pure Al below 100 nm in size. *Acta Materialia*. 2018;152: 138-147.

5. Jia H, Bjørge R, Cao L, Song H, Marthinsen K, Li Y. Quantifying the grain boundary segregation strengthening induced by post-ECAP aging in an Al-5Cu alloy. *Acta Materialia*. 2018;155: 199-213.
6. Shuai LF, Huang TL, Wu GL, Hansen N, Huang X. Characterization of Cu Distribution in an Al-0.3%Cu Alloy Cold Rolled to 98%. *IOP Conf. Series: Materials Science and Engineering*. 2017;219: 012038.
7. Liu Y, Liu M, Chen X, Cao Y, Roven HJ, Murashkin M, Valiev RZ, Zhou H. Effect of Mg on microstructure and mechanical properties of Al-Mg alloys produced by high pressure torsion. *Scripta Materialia*. 2019;159: 137-148.
8. Belov NA, Alabin AN, Matveeva IA, Eskin DG. Effect of Zr additions and annealing temperature on electrical conductivity and hardness of hot rolled Al sheets. *Transactions of Nonferrous Metals Society of China*. 2015;25: 2817-2826.
9. Jiang SY, Wang RH. Manipulating nanostructure to simultaneously improve the electrical conductivity and strength in microalloyed Al-Zr conductors. *Scientific Reports*. 2018;8: 6202.
10. Mavlyutov AM, Orlova TS, Yapparova EKh. The effect of annealing and additional deformation on the mechanical properties of ultrafine-grained Al-1.5Cu alloy. *Technical Physics Letters.* 2020;46: 916-920.
11. Sitdikov VD, Murashkin MY, Valiev RZ, Full-scale use of X-ray scattering techniques to characterize aged Al-2wt.%Cu alloy. *Journal of Alloys and Compounds.* 2018;735: 1792-1798.
12. Nasedkina Y, Sauvage X, Bobruk EV, Murashkin MY, Valiev RZ, Enikeev NA, Mechanisms of precipitation induced by large strains in the Al-Cu system. *Journal of Alloys and Compounds.* 2017;710: 736-747.
13. Orlova TS, Sadykov DI, Murashkin MY, Enikeev NA. Peculiarities of strengthening of Al-Cu-Zr alloy structured by severe plastic deformation. *Physics of the Solid State*. 2021;63: 1744-1756.
14. Orlova TS, Sadykov DI, Danilov DV, Enikeev NA, Murashkin MY. Ultrafine-grained Al-Cu-Zr alloy with high-strength and enhanced plasticity. *Material Letters*. 2021;303: 130490.
15. Orlova TS, Skiba NV, Mavlyutov AM, Murashkin MY, Valiev RZ, Gutkin MY. Hardening by annealing and implementation of high ductility of ultra-fine grained aluminum: experiment and theory. *Reviews on Advanced Materials Science*. 2018;57: 224-240.
16. Gutkin MY, Latynina TA, Orlova TS, Skiba NV. Mechanism of hardening of ultrafine-grained aluminum after annealing. *Physics of the Solid State*. 2019;61: 1790-1799.
17. Skiba NV, Orlova TS, Gutkin MYu. Mechanism of implementation of high ductility in ultrafine-grained aluminum after annealing and subsequent deformation. *Physics of the Solid State*. 2020;62: 2094-2100.
18. Orlova TS, Mavlyutov AM, Gutkin MY. Suppression of the annealing-induced hardening effect in ultrafine-grained Al at low temperatures. *Materials Science Engineering A*. 2021;802: 140588.
19. Gutkin MY, Ovid'ko IA, Skiba NV. Crack-stimulated generation of deformation twins in nanocrystalline metals and ceramics. *Philosophical Magazine*. 2008;88: 1137-1151.
20. Mura T. The continuum theory of dislocations. In: Herman H. (ed.) *Advances in Material Research*. New York: Interscience; 1968. p.1-108.
21. Eshelby JD, Frank FC, Nabarro FRN. XLI. The equilibrium of linear arrays of dislocations. *Philosophical Magazine*. 1951;42: 351-364.
22. Hirth JP, Lothe J. *Theory of Dislocations*. New York: Wiley; 1982.
23. Smithells CJ, Brands EA. *Metals Reference Book*. London: Butterworths, London; 1976.
24. Orlova TS, Latynina TA, Mavlyutov AM, Murashkin MY, Valiev RZ. Effect of annealing on microstructure, strength and electrical conductivity of the pre-aged and HPT-processed Al-0.4Zr alloy. *Journal of Alloys and Compounds.* 2019;784: 41-48.

THE AUTHORS

Skiba N.V.
e-mail: nikolay.skiba@gmail.com
ORCID: 0000-0003-2192-0386

Gutkin M.Yu.
e-mail: m.y.gutkin@gmail.com
ORCID: 0000-0003-0727-6352

Orlova T.S.
e-mail: orlova.t@mail.ioffe.ru
ORCID: 0000-0001-8986-2624